Active and Robust Twisting Morphing Wings With Geometric Constraints for Flying or Swimming Robots

Bing Luo, Weicheng Cui, and Wei Li, *Senior Member, IEEE*

***Abstract*—Typically, a twisting morphing wing of flying or swimming robots has one spanwise shaft and many ribs, the ribs can swing in their individual planes perpendicular to the shaft or the spanwise direction of the wing, showing different swing angles and different speed ratios with respect to the rotation of the shaft, thus the wing can form various degrees of spanwise twisting as the shaft rotates. While feasible solutions and mechanical implementations via gear transmission with tight geometric constraints are largely unexplored. This article considers the tight geometric constraints for such robotic twisting wing, and provides and particularly expands the analytical feasible solutions for the constraints, as well as provides mechanical implementations for active twisting of the wing that is driven by only one motor installed at the wing base, which implementations are compact with low inertia, low control complexity, and also high robustness that tolerates the deformations (e.g., bending due to load) of the shaft. The results serve as a design guidance and can be used for morphing wings of flying or swimming robots, particularly for accurately active spanwise twisting and large load transmissions to the movable parts.**

***Index Terms*—Active torsion, active twisting, morphing wing, robotic wing, twisting morphing wing.**

I. Introduction

A ROBOTIC arm is a type of mechanical arms, with each joint allowing either rotational motion or translational displacement. The wings of some aircraft, robotic birds, or robotic fish with morphing capabilities [1]–[3], [8], [13], [14] can also be viewed as a type of robotic arms. The degrees of freedom are the number of independent motions. Usually, when an independent motion of a joint is expected, an actuator (e.g., a motor) is used; while in many cases, if some joints do not need independent motions or the motions have certain relations with other movable parts, then such motions can be possibly implemented without additional actuators, thus possibly with reduced mechanical and control complexities, as well as with reduced mass inertia and moment of inertia. This article considers such implementations with low inertia, low complexity, and high robustness, which can be applied in, e.g., twisting morphing wings or wing segments of flying or swimming robots [1], [6], [7], [9].

Manuscript received 18 October 2021; accepted 14 December 2021. Date of publication 20 January 2022; date of current version 17 October 2022. Recommended by Technical Editor G. Berselli and Senior Editor W. J. C. Zhang. *(Corresponding author: Wei Li.)*

Bing Luo is with the Department of Mechanics, Zhejiang University, Hangzhou 310027, China, Institute of Advanced Technology, Westlake Institute for Advanced Study, and School of Engineering, Westlake University, Hangzhou 310024, China.

Weicheng Cui and Wei Li are with the Institute of Advanced Technology, Westlake Institute for Advanced Study, and School of Engineering, Westlake University, Hangzhou 310024, China (e-mail: wei.utdallas@live.com).

This article has supplementary material provided by the authors and color versions of one or more figures available at https://doi.org/10.1109/TMECH.2021.3137951.

Digital Object Identifier 10.1109/TMECH.2021.3137951

Twisting (or called torsion [1]) of a morphing wing is effective for control of flying or swimming robots (e.g., flapping flight control, roll control), various methods have been studied to achieve spanwise twisting of morphing wings. For a typical example, SmartBird has active twisting (active torsion) control of each wing to maximize aerodynamic efficiency that is achieved and powered by a motor installed near the wing tip, compared with passive twisting [1], and the twisting distributed along the span is induced by elastic materials; while there is relatively fewer research for morphing wings with accurate twisting along the span and large load transmissions to movable parts [14]. The twist deformation of wings is constructed using lattice-based cellular structures in [3]. A morphing wing in [4] is considered by a twisting tensegrity mechanism. The span extension of wings is considered in [11]. The passive wings of insects are considered in [10]. Aeroelastic structures [12] and shape memory alloys (SMA) [16] are also considered.

In this article, we focus on mechanics of active twisting wings with tight geometric constraints. For a robotic twisting wing (or twisting wing segments, also applicable, e.g., in the scenarios of [1], [6], [7], [9], [19]–[21], [24]), there may exist a spanwise shaft that is driven by a motor and a beam that is fixed and parallel to the shaft to collaboratively support the wing, and there are some ribs that can swing in their individual planes perpendicular to the shaft or the spanwise direction of the wing, showing different swing angles and different speed ratios with respect to the rotation of the shaft, thus the wing can form various degrees of spanwise twisting as the shaft rotates; typically, the ribs near the wing tip have larger swing angles than those near the wing base, similar as wing twisting of birds [17], [19]–[21], and some ribs near the wing tip can be just fixed on the shaft to rotate with the shaft synchronously. The desired specific twisting degrees of the ribs of the wing can be designed by experiments or computational fluid dynamics (CFD) for a specific vehicle with its main operational condition(s), which are outside the scope of this article and omitted here. The skin of the wing is also omitted.

Gear transmission is usually used in robots [22], [23] and is the usual consideration for implementations of mechanical motions, as universal joints [15], which is more accurate and robust for wing morphing than belt (or chain) transmissions [5] or deformations of materials and structures (e.g., SMA [16], elastic, cellular, tensegrity structures [1], [3], [4], [12]). This article considers straight-cut gears that are the typical type of gears, an external gear is the one with the teeth formed on the outer surface of a cylinder, and an internal gear is the one with the teeth formed on the inner surface of a cylinder. For the rib that is not fixed on the shaft, a typical solution is that, a pair of meshing external gear (input gear) and internal gear (output gear) are installed on the shaft and the beam, respectively, for driving this rib (Figs. 1 and 2); the gear fixed on the shaft is used to transmit power from the motor to the rib for its swing motion, the gear on the beam (typically through a rolling bearing and thus not fixed on the beam) is used to support the rib and help transmit power to the rib, with the rib fixed on the output gear. For this pair of gears, the geometric constraints include the *center distance* between

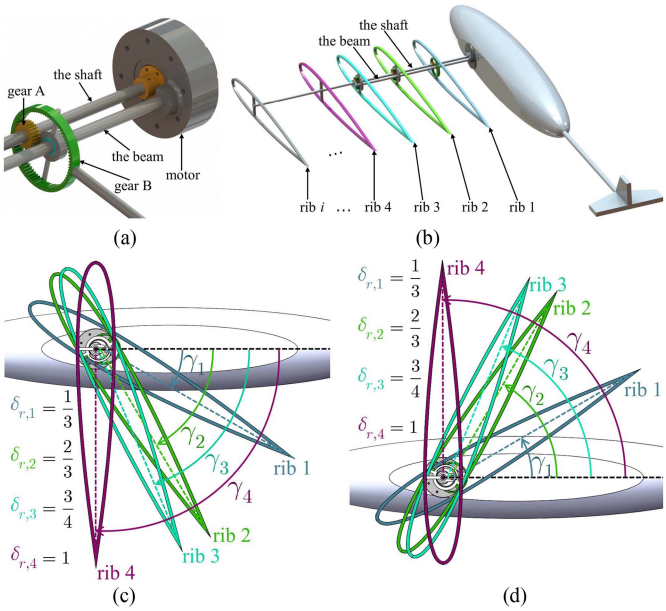

Fig. 1. Illustration of a robotic wing with the morphing capability of spanwise twisting. $\delta_{r,1}=1/3$, $\delta_{r,2}=2/3$, $\delta_{r,3}=3/4$, $\delta_{r,4}=1$. (a) The detailed mechanism with one pair of gears for one rib. (b) Illustration of a whole wing. (c) $\gamma_m=\pi/2$ rad. (d) $\gamma_m=-\pi/2$ rad. A wing may have many ribs that are omitted here. The flapping morphing and the corresponding mechanism of the wing are also omitted here as they are not the focus of this article.

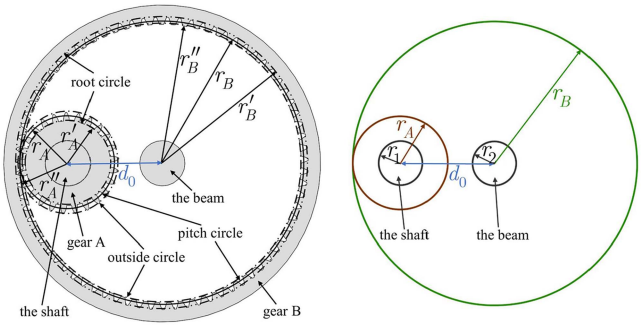

Fig. 2. Illustration of the usual implementation of meshing external gear A and internal gear B. The center of gear A is located at the cross-sectional center of the shaft, the center of gear B is located at the cross-sectional center of the beam.

the shaft and the beam (i.e., the distance between the cross-sectional centers of the shaft and the beam), the radii of the cross-sections of the shaft and the beam, the radii of the pitch circles, root circles, and outside circles of the two gears, as well as the desired or designated speed ratio (gear ratio).

For given values of the center distance between the shaft and the beam, the radii of the cross-sections of the shaft and the beam, then the range of the feasible speed ratios can be determined and is often limited (Figs. 2 and 3). For some speed ratios, usual implementations may be infeasible for tight geometric constraints for some ribs. The mechanical design of gear transmission with the tight geometric constraints and particularly an expansion of the feasible solutions of the constraints thus need to be solved.

The main contributions of this article are as follows. For a twisting morphing wing, since the gear ratios decrease for the ribs from the wing base to the wing tip, thus, in applications, the center distance between the shaft and the beam can be predetermined to satisfy the desired gear

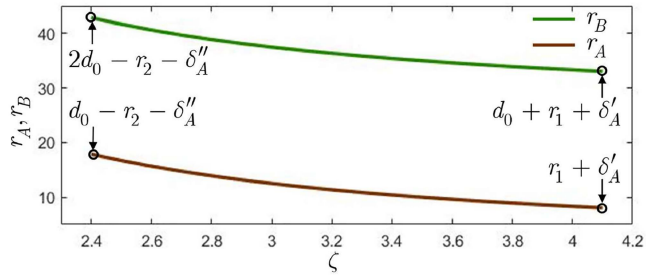

Fig. 3. Feasible values of the radii of the gears and ζ for (5). Here the values of the coordinates show the example with $d_0=25$, $r_1=6$, $r_2=6$, $\delta'_A=2$, $\delta'_B=2$, $\delta''_A=1$, and $\delta''_B=1$.

ratio for the first rib; then, for other ribs, the desired gear ratios may be possibly lower than the feasible range. To solve the tight geometric constraints while not increasing the radii of the gears, we first provide the solution to allow the change of the center distance of each pair of gears to be shorter than the center distance between the shaft and the beam. Then, we provide the analytical feasible solutions (regions) for the gear ratios and the radii of the gears that serve as a design guidance, and we design the corresponding mechanical implementations that are compact with low inertia, low control complexity, and also high robustness that tolerates the deformations (e.g., bending due to load) of the shaft and the beam, which design can be used for morphing wings of flying or swimming robots, particularly for accurately active twisting along the span and large load transmissions to movable parts that may be better than the material-elastic induced twisting along the span for SmartBird [1], and the motor installed at the wing base in this article also has less mass inertia and moment of inertia, compared with the case of the motor installed near the wing tip for SmartBird [1].

The rest of this article is organized as follows: Section II is the problem description. Section III is the analytical feasible solutions of the tight geometric constraints and the mechanical implementations of a twisting morphing wing. Finally, Section IV concludes the article. A supplementary file and a video are also provided.

II. Problem Description

A. Illustration of Spanwise Twisting of a Morphing Wing

An example of a robotic wing with the morphing capability of spanwise twisting is illustrated in Fig. 1 as simple as possible (the flapping morphing is omitted here as it is not the focus of this article). In Fig. 1(a), the motor drives the shaft, which is fixed on the rotor of the motor, thus the motor and the shaft rotate synchronously, a beam that is parallel to the shaft is fixed on the shell of the stator of the motor, rib 1 can swing with angle $\gamma_1 \in \mathbb{R}$ in either the positive or negative direction in the plane that is perpendicular to the shaft, as the motor (i.e., the shaft) rotates with angle $\gamma_m \in \mathbb{R}$, where $\gamma_m \in [-\gamma_0, \gamma_0]$, and $\gamma_0 > 0$. In Fig. 1(c)–(d), there are four ribs that illustrate the spanwise twisting morphing, rib i can swing with angle $\gamma_i \in \mathbb{R}$, $i=1,2,3,4$, in either the positive [Fig. 1(c)] or negative [Fig. 1(d)] direction, as the motor rotates with angle $\gamma_m \in \mathbb{R}$, rib 4 is fixed directly on the shaft. Here the positive direction means the positive pitch angle of the wing. The shaft is used to transmit power from the motor to the ribs. To describe the spanwise twisting, we define $\delta_{r,i} := \gamma_i/\gamma_m \in (0,1]$ as the twist-ratio of rib i. The desired twist-ratios of the ribs can be designed by experiments or CFD for a specific vehicle with its main operational condition(s), which are out the scope of this article and omitted here. Typically, twist-ratios $\delta_{r,i}$ are constant and increase for ribs $i=1,2,\ldots,$ which

show increasingly spanwise twisting of the wing from the wing base to the wing tip.

As the ribs have certain twist-ratios, then such motions can be possibly implemented without additional actuators to reduce mechanical and control complexities, as well as reduce mass inertia and moment of inertia. To achieve $\delta_{r,i}$, consider gear transmission by a pair of meshing gears with an external gear (input gear) fixed on the shaft and an internal gear (output gear) on the beam (typically through a rolling bearing and thus not fixed on the beam), with the rib fixed on the output gear, as in Fig. 2, the external and internal gears are used since $\delta_{r,i} > 0$.

B. Geometric Constraints of the Usual Implementations

The gear ratio, or speed ratio, for a pair of meshing gears is computed as follows: consider input gear A with radius $r_A > 0$ and angular velocity $\omega_A \in \mathbb{R}$ of the pitch circle, output gear B has radius $r_B > 0$ and angular velocity $\omega_B \in \mathbb{R}$ of the pitch circle, the speed of the contact point on the pitch circles is $v = r_A\omega_A = r_B\omega_B \in \mathbb{R}$, the gear ratio is $\zeta := \omega_A/\omega_B \in \mathbb{R}$. For meshing external gear A and internal gear B, as will be used in this article (Fig. 2), the gear ratio is greater than one, i.e.,

$$\zeta := \frac{\omega_A}{\omega_B} = \frac{r_B}{r_A} > 1, \tag{1}$$

which is proportional to the radius of the pitch circle of gear B and inversely proportional to the radius of the pitch circle of gear A. For notations of ith pair of gears, we use subscript i, gear ratio ζ_i is designated as the inverse of the twist-ratio, i.e., $\zeta_i = 1/\delta_{r,i}$, so the gear ratios typically decrease from the wing base to the wing tip. In the following, we consider one pair of gears, and thus, omit the subscript of the notations for clarity.

For external gear A, radius r'_A of the root circle is somewhat smaller than that of the pitch circle, radius r''_A of the outside circle is somewhat greater than that of the pitch circle, i.e., $r''_A > r_A > r'_A$. For internal gear B, radius r'_B of the root circle is somewhat greater than that of the pitch circle, radius r''_B of the outside circle is somewhat smaller than that of the pitch circle, i.e., $r'_B > r_B > r''_B$ (Fig. 2).

The cross-section of the shaft is a circle with radius $r_1 > 0$, the cross-section of the beam is a circle with radius $r_2 > 0$. The center distance between the shaft and the beam is $d_0 > 0$. Usually, r_1, r_2, and d_0 are predetermined, and

$$d_0 > r_1 + r_2. \tag{2}$$

The usual implementation is that the center of gear A is located at the cross-sectional center of the shaft, the center of gear B is located at the cross-sectional center of the beam (so gear A has no confliction with the shaft, gear B has no confliction with the beam). The center distance of the two gears is thus as

$$r_B - r_A = d_0, \tag{3}$$

and from (1), the gear ratio

$$\zeta = 1 + \frac{d_0}{r_A}. \tag{4}$$

Then, the geometric constraints for the pair of the meshing external gear A and internal gear B are as follows (Fig. 2):

$$\begin{cases} \zeta = \frac{r_B}{r_A} > 1, \\ r_B - r_A = d_0 > 0, \\ d_0 - r_2 > r''_A > r_A > r'_A > r_1, \\ r'_B > d_0 + r''_A > r_B > r''_B > d_0 + r'_A \end{cases}$$

for convenience, denote $\delta''_A := r''_A - r_A > 0$, $\delta'_A := r_A - r'_A > 0$, $\delta'_B := r'_B - r_B > 0$, $\delta''_B := r_B - r''_B > 0$; then, in the last inequality, $r'_B > d_0 + r''_A$ means $\delta'_B > \delta''_A$; and $r''_B > d_0 + r'_A$ means $\delta'_A > \delta''_B$. Usually, δ'_A, δ''_A, δ'_B, and δ''_B are very small, compared with the radii of the gears [5]. The geometric constraints for the pair of the gears can also be expressed as follows:

$$\begin{cases} \zeta = \frac{r_B}{r_A} > 1, \\ r_B - r_A = d_0 > 0, \\ r_A \in (r_1 + \delta'_A, d_0 - r_2 - \delta''_A), \\ \delta'_B > \delta''_A > 0, \\ \delta'_A > \delta''_B > 0. \end{cases} \tag{5}$$

Thus, in (5), the range of the gear ratio is

$$\zeta \in \left(1 + \frac{d_0}{d_0 - r_2 - \delta''_A}, 1 + \frac{d_0}{r_1 + \delta'_A}\right). \tag{6}$$

For the values of r_A and r_B, from (1) and (3), we have

$$\begin{cases} r_A = r_A(\zeta) = \dfrac{d_0}{\zeta - 1}, \\ r_B = r_B(\zeta) = \dfrac{d_0\zeta}{\zeta - 1} = d_0 + \dfrac{d_0}{\zeta - 1}. \end{cases} \tag{7}$$

The feasible values of the radii of the gears and ζ for (5) are shown in Fig. 3, without geometric conflictions of the gears with respect to the shaft and the beam.

Example 1: Let $d_0 = 25$, $r_1 = 6$, $r_2 = 6$, $\delta'_A = 2$, $\delta'_B = 2$, $\delta''_A = 1$, $\delta''_B = 1$. The length unit in this article is mm. For $\zeta = 3$ that is in the range of (6), from (7), $r_A = 12.5$ and $r_B = 37.5$.

C. Problem

Consider the pair of the meshing external gear A and internal gear B, given the values of ζ, d_0, r_1, and r_2, with $d_0 > r_1 + r_2$. As for the usual implementations, the center of gear A is located at the cross-sectional center of the shaft, the center of gear B is located at the cross-sectional center of the beam. If a desired or designated gear ratio (e.g., $\zeta = 3/2$ for the parameters of Example 1) is lower than the range of (6), then geometric conflictions exist and such function cannot be achieved by the usual implementation in Section II-B.

Then, for the case that the desired gear ratio is lower than the range of (6), the problems are how to determine and expand feasible solutions of r_A, r_B, ζ, and how to design mechamics for such gear ratios with low inertia, low control complexity, and also high robustness that tolerates the deformations (e.g., bending due to load) of the shaft and the beam?

III. Mechanical Design and Discussion

A. Implementation of a Gear Ratio Lower Than Range (6)

The gear ratios typically decrease for the ribs from the wing base to the wing tip, thus in applications, d_0 is usually first determined to satisfy the desired gear ratio for the first rib, then, for other ribs, the desired gear ratios may be lower than the range of (6). To solve the geometric conflictions of the gears with the shaft and the beam, we consider one solution that is to allow the change of the center distance of the two gears as

$$d := r_B - r_A, \tag{8}$$

where $d \in (0, d_0]$, with a suitable value other than distance d_0.

Remark 1: If we want a desired gear ratio that is greater than the range of (6), we may consider the situation of $d > d_0$, the design procedure and the analytical feasible solutions are similar to those of the situation $d \in (0, d_0]$ in the following of this section, and thus omitted in this article for the limited space.

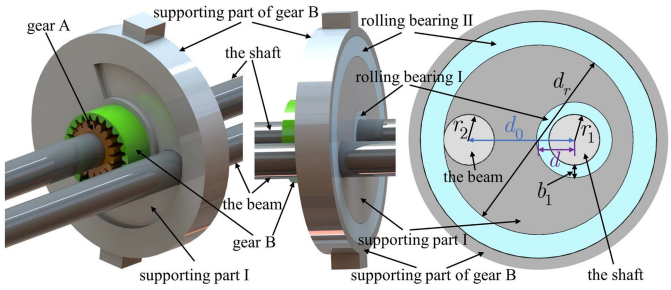

Fig. 4. Example of the mechanical design (from two perspectives) and the geometry. The left side showing the meshing gears. The right side showing the supporting of the gears with the geometry.

For $d \in (0, d_0)$, the center of gear B cannot be located at the cross-sectional center of the beam, the corresponding mechanism needs to be designed with the complexity as simple as possible. Fig. 4 illustrates a mechanical example: One rolling bearing (rolling bearing I) is set on the shaft, its inner ring (or called inner race) is fixed on the shaft and thus rotates synchroneouly with the shaft, its the outer ring (or called outer race) is stationary that is fixed on supporting part I, with the thickness (the difference of the radii of the outer and inner rings) of rolling bearing I as $b_1 > 0$. Supporting part I contains rolling bearing I and the beam, and serves to support another rolling bearing (rolling bearing II). The inner ring of rolling bearing II is fixed on supporting part I and thus is stationary, its outer ring can rotate. The supporting part of gear B is fixed on the out ring of rolling bearing II, thus the teeth of gear B can be set at one side of its supporting part (Fig. 4).

Denote d_r as the diameter of the inner ring of rolling bearing II, d_r should satisfy $d_r \geq d_0 + r_1 + r_2 + b_1$. It is expected to adjust the center of rolling bearing II that is located between the cross-sectional center of the beam and the cross-sectional center of the shaft, with rolling bearing II tightly containing the shaft, rolling bearing I, and the beam. So d_r has the upper limit: $d_r \leq 2(d_0 + \max\{r_1 + b_1, r_2\})$, that is

$$d_r \in [d_0 + r_1 + r_2 + b_1, 2\,(d_0 + \max\{r_1 + b_1, r_2\})] \tag{9}$$

and the relation of d_r and d is

$$d_r = \begin{cases} 2(d_0 + r_2 - d), d \in \left[0, \dfrac{d_0 - r_1 + r_2 - b_1}{2}\right], \\ 2(r_1 + b_1 + d), d \in \left[\dfrac{d_0 - r_1 + r_2 - b_1}{2}, d_0\right]. \end{cases}$$

B. Robustness to Tolerate the Deformations of the Shaft

The mechanical implementations (as illustrated in Figs. 4 and 7, and Supplementary Fig. S1) are also robust to tolerate the deformations of the shaft and the beam due to the following reasons.

1) Supporting part I also has a function to constrain the beam and the shaft to be parallel, and there are typically many such constraints on the wing for the gear ratios that are greater than one; additionally, a bearing pedestal can also be added that is fixed on the end of the beam for parallel constraint of the shaft and the beam that has a similar function of supporting part I.
2) Particularly, the mechanical implementations of the gear transmissions are built directly on supporting part I for each pair of meshing gears, which part can be easily made sufficiently rigid and thus isolate the deformations of the beam and the shaft that are due to external hydrodynamic or aerodynamic loading.

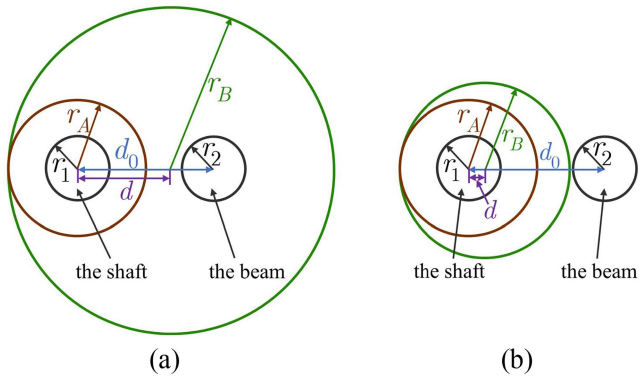

Fig. 5. Geometry of the two gears with the shaft and the beam. (a) The case that the envelop of gear B contains the beam. (b) The case that the envelop of gear B does not contain the beam.

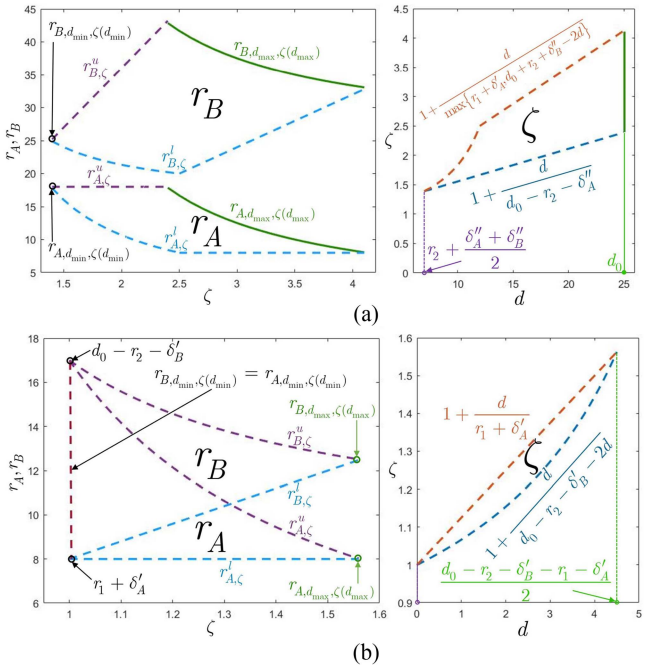

Fig. 6. Illustration of the feasible solutions (regions) of r_A and r_B with respect to ζ, and the feasible region of ζ with respect to d, respectively. Here the values of the coordinates show the example with $d_0 = 25$, $r_1 = 6$, $r_2 = 6$, $\delta'_A = 2$, $\delta'_B = 2$, $\delta''_A = 1$, $\delta''_B = 1$. (a) Feasible regions for inequalities (11) and the range of ζ with respect to d. (b) Feasible regions for inequalities (13) and the range of ζ with respect to d.

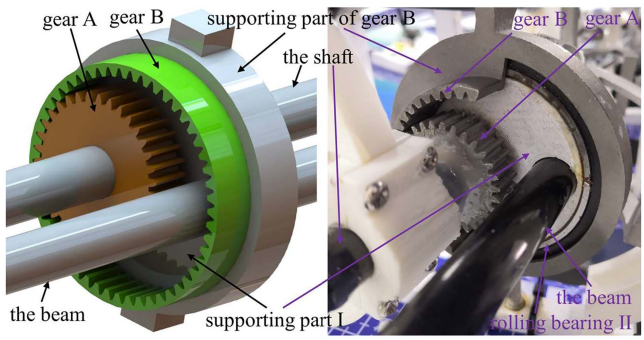

Fig. 7. Mechanical design and implementation of the gear transmission with $\zeta = 3/2$. The left is the CAD model, the right is the physical implementation.

C. Generally Geometric Constraints

Consider the center of gear A that is located at the cross-sectional center of the shaft (thus no confliction with the shaft), the center of gear B can be located between the cross-sectional centers of the shaft and the beam, as with (8), thus, the gear ratio

$$\zeta = 1 + \frac{d}{r_A} > 1. \tag{10}$$

Then, we have the geometric constraints with the two cases:

If the envelop of gear B contains the beam, as Fig. 5(a), then the geometric constraints are as follows:

$$\begin{cases} \zeta = \frac{r_B}{r_A} > 1, \\ d = r_B - r_A \in (0, d_0], \\ r_A \in (r_1 + \delta'_A, d_0 - r_2 - \delta''_A), \\ r_B > d_0 + r_2 + \delta''_B - d, \\ \delta'_B > \delta''_A > 0, \\ \delta'_A > \delta''_B > 0, \end{cases} \tag{11}$$

from the third inequality, $r_A = r_B - d > d_0 + r_2 + \delta''_B - 2d$, and from the second inequality, we have the constraint of the radius of gear A as: $r_A > \max\{r_1 + \delta'_A, d_0 + r_2 + \delta''_B - 2d\} > 0$ and $d_0 - r_2 - \delta''_A > d_0 + r_2 + \delta''_B - 2d$, that is, the range of d and the range of the gear ratio are as follows:

$$\begin{aligned} d &\in \left(r_2 + \frac{\delta''_A + \delta''_B}{2}, d_0\right], \\ \zeta &\in \left(1 + \frac{d}{d_0 - r_2 - \delta''_A}, 1 + \frac{d}{\max\{r_1 + \delta'_A, d_0 + r_2 + \delta''_B - 2d\}}\right). \end{aligned} \tag{12}$$

Here, (11) reduces to be (5), and (12) reduces to be (6), if $d = d_0$; the bounds of (12) are generally lower than that of (6).

If the envelop of gear B does not contain the beam, as in Fig. 5(b), then the geometric constraints are

$$\begin{cases} \zeta = \frac{r_B}{r_A} > 1, \\ d = r_B - r_A \in (0, d_0], \\ r_A \in (r_1 + \delta'_A, d_0 - r_2 - \delta''_A), \\ r_B < d_0 - r_2 - \delta'_B - d, \\ \delta'_B > \delta''_A > 0, \\ \delta'_A > \delta''_B > 0. \end{cases} \tag{13}$$

The third inequality means $r_A = r_B - d < d_0 - r_2 - \delta'_B - 2d$, and notice that $d_0 - r_2 - \delta''_A > d_0 - r_2 - \delta'_B - 2d$ always holds, so $d_0 - r_2 - \delta'_B - 2d > r_1 + \delta'_A$ is required, which means the range of d , so we have

$$\begin{aligned} d &\in \left(0, \frac{d_0 - r_2 - \delta'_B - r_1 - \delta'_A}{2}\right), \\ \zeta &\in \left(1 + \frac{d}{d_0 - r_2 - \delta'_B - 2d}, 1 + \frac{d}{r_1 + \delta'_A}\right). \end{aligned} \tag{14}$$

Here, the values of ζ can be generally smaller than those of (12).

From (8) and (10), we have

$$\begin{cases} r_A = r_A(d, \zeta) = \dfrac{d}{\zeta - 1}, \\ r_B = r_B(d, \zeta) = \dfrac{d\zeta}{\zeta - 1} = d + \dfrac{d}{\zeta - 1}. \end{cases}$$

In the following, we will consider the feasible solutions (regions) of r_A and r_B with respect to ζ for inequalities (11) and inequalities (13), respectively.

D. Feasible Solutions (Regions) of Constraints (11)

Denote the lower and upper boundary curves of r_A as $r^l_{A,\zeta}$ and $r^u_{A,\zeta}$, respectively, denote the lower and upper boundary curves of r_B as $r^l_{B,\zeta}$ and $r^u_{B,\zeta}$, respectively. For inequalities (11) or (13), the feasible solutions (region) of r_A with respect to ζ are contained by the lower, upper, left, and right boundary curves $r^l_{A,\zeta}$, $r^u_{A,\zeta}$, $r_{A,d_{\min},\zeta(d_{\min})}$, and $r_{A,d_{\max},\zeta(d_{\max})}$; the feasible solutions (region) of r_B with respect to ζ are contained by four boundary curves $r^l_{B,\zeta}$, $r^u_{B,\zeta}$, $r_{B,d_{\min},\zeta(d_{\min})}$, and $r_{B,d_{\max},\zeta(d_{\max})}$, with the half-open intervals as

$$\begin{cases} r_A(d,\zeta) \in (r^l_{A,\zeta}, r^u_{A,\zeta}), \\ r_A(d,\zeta) \in \left(r_{A,d_{\min},\zeta(d_{\min})}, r_{A,d_{\max},\zeta(d_{\max})}\right], \\ r_B(d,\zeta) \in (r^l_{B,\zeta}, r^u_{B,\zeta}), \\ r_B(d,\zeta) \in \left(r_{B,d_{\min},\zeta(d_{\min})}, r_{B,d_{\max},\zeta(d_{\max})}\right], \end{cases} \tag{15}$$

where the bounds for inequalities (11) are given as follows:

$$\begin{aligned} r^l_{A,\zeta} &= \max\left\{r_1 + \delta'_A, (d_0 + r_2 + \delta''_B)/(2\zeta - 1)\right\}, \\ r^u_{A,\zeta} &= d_0 - r_2 - \delta''_A, \\ r_{A,d_{\min},\zeta(d_{\min})} &= d_0 - r_2 - \delta''_A, \\ r_{A,d_{\max},\zeta(d_{\max})} &= d_0/(\zeta - 1), \end{aligned}$$

and

$$\begin{aligned} r^l_{B,\zeta} &= \max\left\{(r_1 + \delta'_A)\zeta, (d_0 + r_2 + \delta''_B)\zeta/(2\zeta - 1)\right\}, \\ r^u_{B,\zeta} &= (d_0 - r_2 - \delta''_A)\zeta, \\ r_{B,d_{\min},\zeta(d_{\min})} &= d_0 + (\delta''_B - \delta''_A)/2, \\ r_{B,d_{\max},\zeta(d_{\max})} &= d_0\zeta/(\zeta - 1), \end{aligned}$$

with range ζ given in (12). The feasible solutions (regions) of r_A and r_B with respect to ζ are illustrated in Fig. 6(a).

Remark 2: Here, $r^l_{A,\zeta}$ is derived from $d = r^l_{A,\zeta}(\zeta - 1)$ and $r^l_{A,\zeta} = \max\{r_1 + \delta'_A, d_0 + r_2 + \delta''_B - 2r^l_{A,\zeta}(\zeta - 1)\}$; $d_{\max} = d_0$; $d_{\min} = r_2 + (\delta''_A + \delta''_B)/2$; while $r_{A,d_{\min},\zeta(d_{\min})}$ and $r_{B,d_{\min},\zeta(d_{\min})}$ reduce to be two points, since the lower and upper bounds of $\zeta(d_{\min})$ for $d = d_{\min}$ are equal as $1 + (2r_2 + \delta''_A + \delta''_B)/(2(d_0 - r_2 - \delta''_A))$.

E. Feasible Solutions (Regions) of Constraints (13)

For inequalities (13), the feasible solutions (regions) of r_A and r_B with respect to ζ are given by

$$\begin{cases} r_A(d,\zeta) \in (r^l_{A,\zeta}, r^u_{A,\zeta}), \\ r_A(d,\zeta) \in \left(r_{A,d_{\min},\zeta(d_{\min})}, r_{A,d_{\max},\zeta(d_{\max})}\right), \\ r_B(d,\zeta) \in (r^l_{B,\zeta}, r^u_{B,\zeta}), \\ r_B(d,\zeta) \in \left(r_{B,d_{\min},\zeta(d_{\min})}, r_{B,d_{\max},\zeta(d_{\max})}\right), \end{cases} \tag{16}$$

which has only open intervals, and in which the bounds are

$$\begin{aligned} r^l_{A,\zeta} &= r_1 + \delta'_A, \\ r^u_{A,\zeta} &= (d_0 - r_2 - \delta'_B)/(2\zeta - 1), \\ r_{A,d_{\min},\zeta(d_{\min})} &= (r_1 + \delta'_A, d_0 - r_2 - \delta'_B), \\ r_{A,d_{\max},\zeta(d_{\max})} &= r_1 + \delta'_A, \end{aligned}$$

and

$$\begin{aligned} r^l_{B,\zeta} &= (r_1 + \delta'_A)\zeta, \\ r^u_{B,\zeta} &= (d_0 - r_2 - \delta'_B)\zeta/(2\zeta - 1), \\ r_{B,d_{\min},\zeta(d_{\min})} &= (r_1 + \delta'_A, d_0 - r_2 - \delta'_B), \\ r_{B,d_{\max},\zeta(d_{\max})} &= (d_0 - r_2 - \delta'_B + r_1 + \delta'_A)/2. \end{aligned}$$

The feasible solutions (regions) of r_A and r_B with respect to ζ are illustrated in Fig. 6(b).

Remark 3: Here, $d_{\max} = (d_0 - r_2 - \delta'_B - r_1 - \delta'_A)/2$; $r^u_{A,\zeta}$ is derived from $r^u_{A,\zeta} = d_0 - r_2 - \delta'_B - 2r^u_{A,\zeta}(\zeta - 1)$; notice that $d_{\min} = 0$ for $r_{A,d_{\min},\zeta(d_{\min})} = r_{B,d_{\min},\zeta(d_{\min})} = (r_1 + \delta'_A, d_0 - r_2 - \delta'_B)$, which represents a vertical line segment for $\zeta = 1$; and $d_{\max} = (d_0 - r_2 - \delta'_B - r_1 - \delta'_A)/2$, thus, the lower and upper bounds of

$\zeta(d_{\max})$ are equal as $1+(d_0-r_2-\delta'_B-r_1-\delta'_A)/(2(r_1+\delta'_A))$, so $r_{A,d_{\max},\zeta(d_{\max})}$ and $r_{B,d_{\max},\zeta(d_{\max})}$ reduce to be two points.

Remark 4: From Section III-C and D, for a same value of ζ, there exist a range of feasible values of d, and thus, the ranges of feasible values of r_A and r_B, which are flexible for design.

Example 2: In Example 1, let $\zeta = 4/3$, from (14), for $d = 3$, then $r_A = 9$, $r_B = 12$, as illustrated in Fig. 4. While in Example 1, let $\zeta = 3/2$, from (12), for $d = 8.5$, then $r_A = 17, r_B = 25.5$, as in Fig. 7.

There are also two physical implementations illustrated in Supplementary Fig. S3, due to the limited space here.

IV. Conclusion

This article considers the tight geometric constraints and mechanical design for active spanwise wing twisting. The analytical feasible solutions of the constraints are provided and expanded that serve as a design guidance, and the mechanical implementations are provided that are compact and robust for morphing wings, particularly for accurately active spanwise twisting and large load transmissions to the movable parts.

There are some future considerations, e.g., the skin design with elastic materials and a prototype vehicle with the wings will be experimented together with morphing control; the computations of the shear force and bending moment on the shaft, and design of spanwise bending morphing with a degree of freedom and chordwise morphing of the wing (e.g., each rib with some segments [18]) will also be considered in future.

References

[1] D. Mackenzie, "A flapping of wings," *Science*, vol. 335, pp. 1430–1433, 2012.

[2] M. Di Luca, S. Mintchev, G. Heitz, F. Noca, and D. Floreano, "Bioinspired morphing wings for extended flight envelope and roll control of small drones," *Interface Focus*, vol. 7, 2017, Art. no. 20160092.

[3] B. Jenett *et al.*, "Digital morphing wing: Active wing shaping concept using composite lattice-based cellular structures," *Soft Robot*, vol. 4, no. 1, pp. 33–48, 2017.

[4] N. K. Pham and E. A. P. Hernandez, "Modeling and design exploration of a morphing wing enabled by a twisting tensegrity mechanism,"*AIAA Scitech Forum*, Jan. 2021, Art. no. 2021–0099.

[5] N. Gorkaneshan, B. Varadarajan, and C. B. Senthil Kumar, *Mechanics and Calculations of Textile Machinery*. New Delhi, India: WPI Publishing, 2012.

[6] J. S. Izraelevitz and M. S. Triantafyllou, "A novel degree of freedom in flapping wings shows promise for a dual aerial/aquatic vehicle propulsor," in *Proc. IEEE Int. Conf. Robot. Autom.*, Jul. 2015, pp. 5830–5837.

[7] H. Rodrigue *et al.*, "Effect of twist morphing wing segment on aerodynamic performance of UAV," *J. Mech. Sci. Technol.*, vol. 30, no. 1, pp. 229–236, 2016.

[8] B. A. Roccia, S. Preidikman, M. L. Verstraete, and D. T. Mook, "Influence of spanwise twisting and bending on lift generation in MAV-like flapping wings," *J. Aerosp. Eng.*, vol. 30, no. 1, 2017, doi: 10.1061/(ASCE)AS.1943-5525.0000677.

[9] S. A. Fazelzadeh, M. Rezaei, and A. Mazidi, "Aeroelastic analysis of swept pre-twisted wings," *J. Fluids Struct.*, vol. 95, 2020, Art. no. 103001.

[10] H. V. Phan, Q. T. Truong, and H. C. Park, "An experimental comparative study of the efficiency of twisted and flat flapping wings during hovering flight," *Bioinspir. Biomim.*, vol. 12, 2017, Art. no. 036009.

[11] R. M. Ajaj *et al.*, "Span morphing using the GNATSpar wing," *Aerosp. Sci. Technol.*, vol. 53, pp. 38–46, 2016.

[12] N. B. Cramer *et al.*, "Elastic shape morphing of ultralight structures by programmable assembly," *Smart Mater. Struct.*, vol. 28, 2019, Art. no. 055006.

[13] R. M. Ajaj, M. I. Friswell, W. G. Dettmer, G. Allegri, and A. T. Isikveren, "Dynamic modelling and actuation of the adaptive torsion wing," *J. Intell. Mater. Syst. Struct.*, vol. 24, pp. 2045–2057, 2013.

[14] S. Ameduri and A. Concilio, "Morphing wings review: Aims, challenges, and current open issues of a technology," *Proc IMechE Part C*, 2020.

[15] S. R. Hummel and C. Chassapis, "Configuration design and optimization of universal joints with manufacturing tolerances," *Mech. Mach. Theory*, vol. 35, pp. 463–476, 2000.

[16] S. Ameduri, A. Brindisi, B. Tiseo, A. Concilio, and R. Pecora, "Optimization and integration of shape memory alloy (SMA)-based elastic actuators within a morphing flap architecture," *J. Intell. Mater. Syst. Struct.*, vol. 23, no. 4, pp. 381–396, 2012.

[17] M. Maeda, T. Nakata, I. Kitamura, H. Tanaka, and H. Liu, "Quantifying the dynamic wing morphing of hovering hummingbird," *R. Soc. Open Sci.,* vol. 4, 2017, Art. no. 170307.

[18] G. Jodin *et al.*, "Optimized design of real-scale A320 morphing high-lift flap with shape memory alloys and innovative skin," *Smart Mater. Struct.*, vol. 27, 2018, Art. no. 115005.

[19] M. Fluck and C. Crawford, "A lifting line model to investigate the influence of tip feathers on wing performance," *Bioinspir. Biomim.*, vol. 9, 2014, Art. no. 046017.

[20] G. Iosilevskii, "Forward flight of birds revisited. Part 1: Aerodynamics and performance," *R. Soc. Open Sci.*, vol. 1, 2014, Art. no. 140248.

[21] P. Henningsson, A. Hedenstrom, and R. J. Bomphrey, "Efficiency of lift production in flapping and gliding flight of swifts," *PLoS ONE*, vol. 9, no. 2, 2014, Art. no. e90170.

[22] H. Matsuki, K. Nagano, and Y. Fujimoto, "Bilateral drive gear—A highly backdrivable reduction gearbox for robotic actuators," *IEEE/ASME Trans. Mechatronics*, vol. 24, no. 6, pp. 2661–2673, Dec. 2019.

[23] S. Crispel *et al.*, "A novel Wolfrom-based gearbox for robotic actuators," *IEEE/ASME Trans. Mechatronics*, vol. 26, no. 4, pp. 1980–1988, Aug. 2021.

[24] Y. Shen, N. Harada, S. Katagiri, and H. Tanaka, "Biomimetic realization of a robotic penguin wing: Design and thrust characteristics," *IEEE/ASME Trans. Mechatronics*, vol. 26, no. 5, pp. 2350–2361, Oct. 2021.